Dispersion relation for surface plasmon polaritons on a Schottky junction

Thamani Wijesinghe[1,*] **and Malin Premaratne**[1]

[1]*Advanced Computing and Simulation Laboratory (AχL), Department of Electrical and Computer Systems Engineering, Monash University, Clayton, Victoria 3800, Australia*

[*]*thamani.wijesinghe@monash.edu*

Abstract: The conventional analysis of surface plasmon modes on dielectric–metal interfaces requires clearly defining the permittivity discontinuity at the interface. A pivotal assumption of such an analysis is that the formation of the dielectric-metal interface does not change the material properties and the materials forming the interface have identical permittivities before and after the formation of the interface. However, this assumption breaks down if an interface is made between a metal and a semiconductor which is commonly known as a Schottky junction. Under certain conditions, such an interface can sustain a surface plasmon polariton (SPP) mode. It is also possible to change the properties of the media surrounding the Schottky junction interface by applying an external potential difference across the junction. Central to the understanding of the SPP mode behaviour in such a complex morphological interface is the dispersion relation which defines the feasible SPP modes and their characteristics. Here, we carry out a detailed analysis to derive an analytical expression for the dispersion relation for a Schottky junction. Our analysis takes into account the space charge layer formed due to the charge distribution across the Schottky junction and resulting new boundary conditions.

OCIS codes: (240.6680) Surface plasmons; (250.5403) Plasmonics.

References and links

1. M. Premaratne and G. P. Agrawal, *Light Propagation in Gain Media: Optical Amplifiers* (Cambridge University Press, 2011).
2. W. L. Barnes, A. Dereux, and T. W. Ebbesen, "Surface plasmon subwavelength optics," Nat. Photonics **424,** 824–830 (2003).
3. D. Sarid and W. Challener, *Modern Introduction to Surface Plasmons: Theory, Mathematica Modeling and Applications* (Cambridge University Press, 2010).
4. S. A. Maier, *Plasmonics: Fundamentals and Applications* (Springer Science, 2007).
5. G. V. Naik and A. Boltasseva, "Semiconductors for Plasmonics and Metamaterials," Phys. Status Solidi (RRL) **4,** 295–297 (2010).
6. R. T. Holm and E. D. Palik, "Surface plasmons in semiconductor-insulator multilayers," CRC Crit. Rev. Sol. State Mat. Sci., 397–404 (2006).
7. A. V. Krasavin and A. V. Zayats, "Silicon-based plasmonic waveguides," Opt. Express **18,** 11791–11799 (2010).
8. K. H. Aharonian and D. R. Tilley, "Propagating electromagnetic modes in thin semiconductor films," J. Phys.: Condens. Matter I, 5391–5401 (1989).
9. S. A. Maier, "Gain-assisted propagation of electromagnetic energy in subwavelength surface plasmon polariton gap waveguides," Opt. Commun. **258,** 295–299 (2006).
10. D. Handapangoda, I. D. Rukhlenko, M. Premaratne, and C. Jagadish, "Optimization of gain–assisted waveguiding in metal–dielectric nanowires," Opt. Lett. **35,** 4190–4192 (2010).

#161732 - $15.00 USD Received 18 Jan 2012; revised 28 Feb 2012; accepted 5 Mar 2012; published 13 Mar 2012

11. D. Y. Fedyanin and A. V. Arsenin, "Surface plasmon polariton amplification in metal-semiconductor structures," Opt. Express **19,** 12524–12531 (2011).
12. I. B. Udagedara, I. D. Rukhlenko, and M. Premaratne, "Complex–ω approach versus complex–**k** approach in description of gain–assisted SPP propagation along linear chains of metallic nano spheres," Phys. Rev. B **83,** 115451 (2011).
13. I. B. Udagedara, I. D. Rukhlenko, and M. Premaratne, "Surface plasmon–polariton propagation in piecewise linear chains of nanospheres: The role of optical gain and chain layout," Opt. Express **19,** 19973–19986 (2011).
14. M. S. Kushwaha, "Plasmons and magnetoplasmons in semiconductor heterostructures," Surf. Sci. Rep. **41,** 1–416 (2001).
15. A. Yariv and R. C. C. Leite, "Dielectric waveguide mode of light propagation in p-n junctions," Appl. Phys. Lett. **2,** 55–57 (1963).
16. R. F. Wallis, J. J. Brion, E. Burstein, and A. Hartstein, "Theory of surface polaritons in semiconductors," in *Proceedings of the Eleventh International Conference on the Physics of Semiconductors*, (Elsevier 1972) 1448–1453.
17. J. C. Inkson, "Many-body effects at metal-semiconductor junctions. I. Surface plasmons and the electron-electron screened interaction," J. Phys. C: Solid State Phys. **5,** 2599–2610 (1972).
18. L. Solymar and D. Walsh, *Electrical Properties of Materials* (Oxford University Press, 2004).
19. K. F. Brennan, *Introduction to Semiconductor Devices: For Computing and Telecommunications Applications* (Cambridge University Press, 2005).
20. S. L. Cunningham, A. A. Maradudin, and R. F. Wallis, "Effect of a charge layer on the surface-plasmon-polariton dispersion curve ," Phys. Rev. B **10,** 3342–3355 (1974).
21. C. C. Kao and E. M. Conmell, "Surface plasmon dispersion of semiconductors with depletion or accumulation layers," Phys. Rev. B **14,** 2464–2479 (1976).
22. N. Lebedev and R. A. Silverman, *Special Functions and Their Applications* (Dover Publication, 1972).
23. S. S. Bayin, *Mathematical Methods in Science and Engineering* (Wiley–Interscience, 2006).
24. E. N. Economou, "Surface Plasmons in Thin Films," Phys. Rev. Lett. **182,** 539–554 (1969).
25. P. Halevi, "Electromagnetic wave propagation at the interface between two conductors," Phys. Rev. B **12,** 4032–4035 (1975).
26. H. C. Casey and M. B. Panish, *Heterostructure Lasers, Part A: Fundamental Principles* (Academic, 1978).
27. D. Y. Fedyanin, "Toward an electrically pumped spaser," Opt. Lett. **37,** 404–406 (2012).

1. Introduction

Surface plasmon polartions (SPPs) are hybrid transverse magnetic optical waves that are bounded and propagate along metal–dielectric interfaces and oscillate collectively with free electrons in the metal [1]. The ability of metal–dielectric interfaces and metal nano structures to localize and manipulate SPP modes at nano scale have opened up intensive research avenues in areas such as photonics and integrated optics, biomedical imaging, molecular sensing and spectroscopy [2–4]. The new capabilities of SPP are being explored using various structures ranging from simple metal–dielectric interfaces to complex nano structures consisting of semiconductor-dielectric interfaces, enabling inter-operability and integration with existing semiconductor technology. The enhanced performance of plasmonic structures are achieved by modifying a simple metal–dielectric interface into multi layered structures or by modifying the metal geometry itself, which include metal grooves, ridges or changing the properties of the medium [5–8].

SPP has been widely studied for many decades to understand the physics behind the phenomena and to extend the knowledge towards device applications. But it was only recently the interest grew towards gain assisted SPP amplification to overcome high propagation losses experienced in plasmonic structures [9–13]. Among plethora of technologies available for providing gain for SPPs, one promising approach is the replacement of passive dielectric material by a semiconductor and use electrical pumping to achieve gain [11]. So, there is great need to have a clear understanding of the behaviour of SPPs on semiconductor– metal junctions. Even though there are a large number of papers analysing the SPP behaviour on metal–dielectric interfaces [1, 4], the associated results cannot be directly ported to semiconductor–metal interfaces. This is mainly due the reason that the conventional analysis of surface plasmon modes on metal–dielectric interfaces rely on knowing the exact value of permittivity at either side of

#161732 - $15.00 USD Received 18 Jan 2012; revised 28 Feb 2012; accepted 5 Mar 2012; published 13 Mar 2012

the interface [1]. A pivotal assumption of such an analysis is that the formation of the metal–dielectric interface does not change the material properties and the materials forming the interface have identical permittivities before and after the formation of the interface [4].

However, this assumption breaks down if an interface is made between a metal and a semiconductor, which is commonly known as a Schottky junction. The properties of Schottky junction interface predominantly depends on the size and shape of the interface, doping density of impurities in the semiconductor medium and type and quality of the metal [14]. Interestingly, some of these interface properties of the Schottky junction can be changed by applying an external potential difference across the junction. It is this potent property of Schottky junctions makes it very attractive for modern plasmonic applications. Later we show that under certain conditions, such an interface can sustain one or two surface plasmon polariton (SPP) mode/s. Central to the understanding of the SPP mode behaviour in such a complex morphological interface is the dispersion relation which defines the feasible SPP modes and their characteristics [1, 4]. The analysis demands special care because, unlike in a metal–dielectric interface, a region of nonuniform free charge carrier density profile develops surrounding a metal–semiconductor interface. The width of this region is in the range of hundreds of nanometers. This substantial variations in the free charge density in the vicinity of the metal–semiconductor interface influence the permittivity seen by the SPP wave propagating along the interface. Moreover, such charge variations may give rise to energy confinement at the junction and severely constrain the features of electromagnetic waves that can collectively oscillate with the free electron plasma [15–17].

In this paper, we carry out a detailed analysis to derive an analytical expression for the dispersion relation for a Schottky junction and show that a very good agreement exists between analytical and numerical dispersion relations. Our analysis takes into account the space charge layer formed due to the charge distribution across the Schottky junction and resulting new boundary conditions. Unlike in a dielectric–metal interface where a single SPP mode is supported, we show that the solution of the new analytical dispersion relation correctly predicts two SPP modes of low energy and high energy, which have already observed in bi-metallic systems experimentally. Moreover, SPP mode behaviour under various charge density profiles, varying external potential and different metals (e.g. Au, Ag, Al and Cu) are presented. This paper is organized as follows. In Section 2, we outline an analytical description of Schottky junction and derive the characteristic equations for the existence of plasmon modes in a model four layered system introducing new boundary conditions for space charge layer. Section 3 describes the numerical solution for the SPP dispersion relation of the junction. The effect of system parameters on dispersion characteristics are also examined. Section 4 concludes this paper after summarising the main result and emphasizing the importance of this study.

2. Characterization of the surface plasmon field at the Schottky junction

The metal–semiconductor contact creates a hetero-interface (widely called a Schottky junction) and consists of a space charge region with a varying free charge carrier density profile formed according to the band structure of the semiconductor and the metal [18, 19]. In electronics engineering, junctions play an important role because of their ability to rectify currents, which is a direct result of having a space charge layer on the semiconductor side of the interface. In this section, we briefly describe the junction properties and associated charge distribution before deriving an analytical expression for the dispersion relation for the SPP modes propagating along the vicinity of the Schottky junction interface.

#161732 - $15.00 USD Received 18 Jan 2012; revised 28 Feb 2012; accepted 5 Mar 2012; published 13 Mar 2012

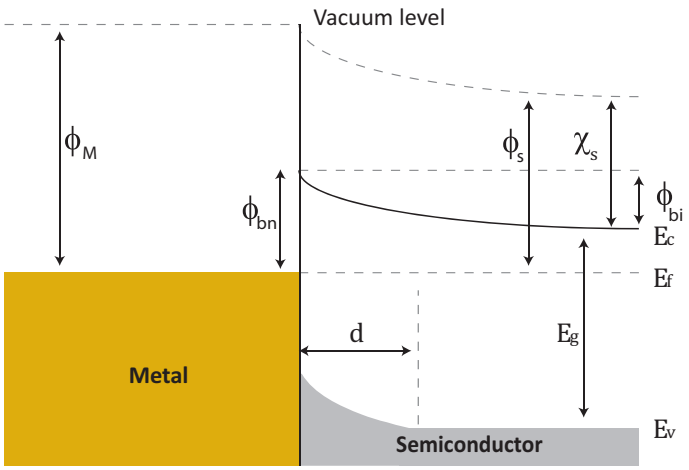

Fig. 1. The energy band diagram of a metal and n–type semiconductor junction in equilibrium. The work functions are denoted by ϕ_M ad ϕ_s where $\phi_M > \phi_s$ and χ_s denotes electron affinity of the semiconductor.

2.1. *Description of the metal-semiconductor junction*

To introduce the notation used and the major parameters considered in our model, this section briefly defines the intrinsic and extrinsic parameters of the Schottky junction. The band structure for a metal and n-Semiconductor contact is shown in Fig. 1. Here E_f is the Fermi energy level and E_c, E_v are the conduction and valence band edges, respectively. The built in potential across the depletion layer ϕ_{bi} is given by,

$$q\phi_{bi} = q\phi_{bn} - (E_c - E_F) = q\phi_{bn} - V_T \ln \frac{N_c}{N_d}$$

where ϕ_{bn}, N_c, N_d and V_T denote Schottky barrier height, effective density of states in the conduction band, doping concentration of semiconductor and thermal voltage. We can apply full depletion approximation to find the width of the space charge region when an external voltage V_A is applied across the junction [19],

$$d = \tau \sqrt{\frac{2\varepsilon_s(\phi_{bi} - V_A)}{qN_d}}. \tag{1}$$

Here τ is a parameter which depends on the surface characteristics of the semiconductor. Accordingly, for Si-Au and Si-Ag contacts, width of the space charge layer assumed to be in the range of $0.1 \sim 1\ \mu m$ for doping concentration around $10^{28} m^{-3}$.

2.2. *Analytical estimation of the plasmonic field distribution*

The dispersion characteristics of plasmon modes at a semiconductor–vacuum interface has been studied by Wallis *et al*. under the approximation in which the space charge layer is represented by a piecewise linear variation [16,20]. Even though several attempts have been made to replace this linear variation assumption by much smoother transition (e.g. for exponential profile see [21].), no substantial improvements can be gained but lead to complex set of equations that are hard to solve [21]. As our prime aim of this paper is to obtain an analytical result for

#161732 - $15.00 USD Received 18 Jan 2012; revised 28 Feb 2012; accepted 5 Mar 2012; published 13 Mar 2012

the dispersion relation, without loss of generality, we assume a piecewise linear variation of the charge profile in the subsequent analysis [20]. However, it must be emphasised that any complex profile can always be approximated by a reasonably chosen piecewise linear variation and thus the fundamental does not allude a limitation of our analysis.

In this context, the Schottky Junction is represented by four layers as shown in Fig. 2. The structure consisting a semi-infinite semiconductor film in contact with a semi-infinite metal. The dielectric function for both media is defined by the lossless Drude model in the absence of interband transitions as given below,

$$\varepsilon_\zeta(z,\omega) = \varepsilon_{H\zeta}\left[1-\frac{\omega_{p\zeta}^2}{\omega^2}\right], \qquad \zeta \in \{m,s\} \tag{2}$$

where the indexes m and s refer to metals and semiconductors, respectively. $\varepsilon_{H\zeta}, \zeta \in \{m,s\}$ is the static dielectric constant of the medium and $\omega_{p\zeta}, \zeta \in \{m,s\}$ is the plasma frequency of the medium. It is important to note that for a metal $\varepsilon_{Hm} = 1$ and for a semiconductor $\omega_{ps}^2(z) = 4\pi q^2 n(z)/(\varepsilon_{Hs} m^*) \equiv \omega_{ps0}^2 n(z)/n_b$, where n_b is a reference cross-sectional carrier density to be defined later and $\omega_{ps0}^2 = 4\pi q^2 n_b/(\varepsilon_{Hs} m^*)$. Here q and m^* are the magnitude of electron charge and the effective mass of charge carrier, respectively and $n(z)$ is the position dependent free charge carrier density. Depending on the value of $n(z)$, the junction can be divided into four region as shown in Fig. 2. In the regions **A** , **B** and **D**, $n(z)$ is spatially constant. In the region **C**, $n(z)$ is approximated by a linear variation as given below [20].

$$n(z) = n_b(rz+\varsigma). \tag{3}$$

Here r and ς denote the slope and vertical intersect of the linear function. Substitution of Eq. (3) to Eq. (2) enables us to write the dielectric constant in the region **C** as

$$\varepsilon_s(z,\omega) = -\frac{\varepsilon_{Hs} r \omega_{ps0}^2}{\omega^2}(z-z_0)$$

where $z_0 = (\omega^2/\omega_{ps0}^2 - \varsigma)/r$. With the definition of these new variables, we can summarise the permittivity of the **A**, **B**, **C** and **D** sections of Fig. 2 as follows:

$$\text{region } \mathbf{A}: \quad z \le 0, \qquad \varepsilon_{mA}(z,\omega) = 1-\frac{\omega_{pm}^2}{\omega^2} \tag{4a}$$

$$\text{region } \mathbf{B}: \quad 0 < z \le d_1 \qquad \varepsilon_{sB}(z,\omega) = \varepsilon_{Hs} \tag{4b}$$

$$\text{region } \mathbf{C}: \quad d_1 < z \le d_2 \qquad \varepsilon_{sC}(z,\omega) = -\frac{\varepsilon_{Hs} r \omega_{ps0}^2}{\omega^2}(z-z_0) \tag{4c}$$

$$\text{region } \mathbf{D}: \quad d_2 < z \qquad \varepsilon_{sD}(z,\omega) = \varepsilon_{Hs}\left[1-\frac{\omega_{ps0}^2}{\omega^2}\right] \tag{4d}$$

Even though there is a possibility to have both TE and TM SPP modes to propagate along the junction in x axis of the Fig. 2, application of the Maxwell's equations with proper boundary conditions to the bounded mode at the junction shows that only the TM modes are supported [4]. For such a TM mode, only the components E_x, H_y and E_z are non-zero. Noting that these components propagate along the $+x$ direction, we can write

$$E_\nu(x,z,t) = E_\nu(z)\exp(ikx - i\omega t), \qquad \nu \in \{x,z\},$$

where k is the longitudinal wave number along the direction x and $E_\nu(z)$ is the amplitude of $E_\nu(x,z,t)$ where $\nu \in \{x,z\}$. For these TM modes, the Maxwell's equations give the following

#161732 - $15.00 USD Received 18 Jan 2012; revised 28 Feb 2012; accepted 5 Mar 2012; published 13 Mar 2012

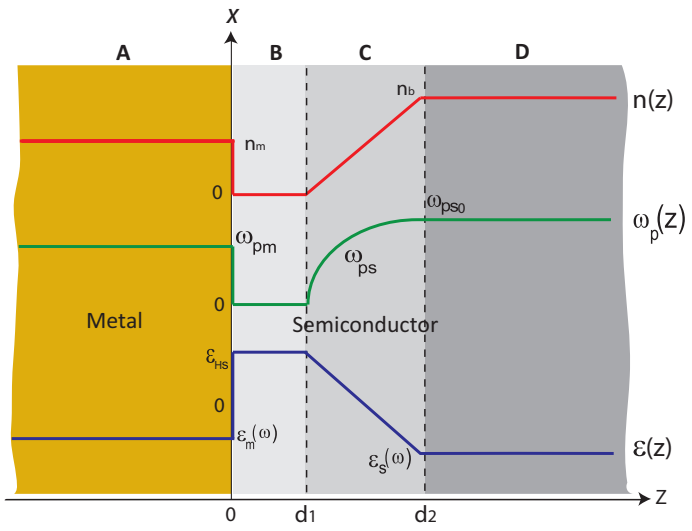

Fig. 2. A Schematic illusion of the Schottky Junction including the division of the junction to sections **A**, **B**, **C**, and **D** based on the carrier density distribution.

set of partial differential equations for the electric field components if the external charges and currents are absent in the medium,

$$\nabla \times \nabla \times (E_x(x,z,t)\hat{\mathbf{x}} + E_z(x,z,t)\hat{\mathbf{z}}) = -\frac{\varepsilon(z,\omega)}{c^2}\frac{\partial^2}{\partial t^2}(E_x(x,z,t)\hat{\mathbf{x}} + E_z(x,z,t)\hat{\mathbf{z}})$$

where $\hat{\mathbf{x}}$ and $\hat{\mathbf{z}}$ are the unit vectors in the x, z directions, respectively and $\varepsilon(z,\omega)$ is the local permittivity of the medium as specified in Eq. (4). It is much more useful if these equations are written using their component form. Collecting and matching terms in $\hat{\mathbf{x}}$ and $\hat{\mathbf{z}}$ directions gives

$$ik\frac{\partial E_z(z)}{\partial z} - \frac{\partial^2 E_x(z)}{\partial z^2} = \frac{\omega^2\varepsilon(z,\omega)}{c^2}E_x(z) \tag{5a}$$

$$ik\frac{\partial E_x(z)}{\partial z} + k^2 E_z(z) = \frac{\omega^2\varepsilon(z,\omega)}{c^2}E_z(z) \tag{5b}$$

To solve these simultaneous partial differential equations, it is better to eliminate one dependent variable. We choose to eliminate the $E_x(z)$ from the Eq. (5a). This can be done by taking the derivative of Eq. (5b) with respect to z and substitution of the resulting equation in Eq. (5a). The resulting second order partial differential equation reads

$$\begin{aligned}\frac{\partial^2 E_z(z)}{\partial z^2} + \frac{\partial \ln(\varepsilon(z,\omega))}{\partial z}\frac{\partial E_z(z)}{\partial z} \\ - \left[k^2 - \frac{\omega^2\varepsilon(z,\omega)}{c^2} - \frac{1}{\varepsilon(z,\omega)}\frac{\partial^2\varepsilon(z,\omega)}{\partial z^2} + \left(\frac{1}{\varepsilon(z,\omega)}\frac{\partial\varepsilon(z,\omega)}{\partial z}\right)^2\right]E_z(z) = 0\end{aligned} \tag{6}$$

Once found, this solution can be used to calculate the $E_x(z)$ component from the following relation obtained using Eq. (5a) and Eq. (5b).

$$E_x(z) = \frac{i}{k}\left(\frac{\partial E_z(z)}{\partial z} + \frac{\partial \ln(\varepsilon(z,\omega))}{\partial z}E_z(z)\right) \tag{7}$$

#161732 - $15.00 USD Received 18 Jan 2012; revised 28 Feb 2012; accepted 5 Mar 2012; published 13 Mar 2012

This equation assumes different forms depending on the permittivity of regions **A**, **B**, **C** and **D** given in Eq. (4). Because the solution and the format of the equation change in each of these sections, we solve the above equation for each section separately below. It is important to notice that we need these solutions at each section because the dispersion relation applicable to Schottky junction is obtained by ensuring the continuity conditions of the field components as described later.

(i) Solution of Eq. (6) *in region* **A** *where* $z \leq 0$ *:*

Here the dielectric function is spatially constant (see Eq. (4a)) and hence Eq. (6) assumes the following simple form:

$$\frac{\partial^2 E_z}{\partial z^2} + (k_0^2 \varepsilon_{mA} - k^2) = 0 \tag{8}$$

Once found this solution, we can get $E_x(z)$ using the Eq. (7) where the second term goes to zero because of the permittivity is constant in the region **A**.

$$E_x(z) = \frac{i}{k} \frac{\partial E_z}{\partial z} \tag{9}$$

The solution of the Eq. (8) is well-known and can be written directly as

$$E_z(z) = E_A \exp(\beta_A z), \qquad \beta_A \in \mathbb{R}_{>0} \tag{10}$$

where E_A is a constant and the longitudinal wave vector is given by $\beta_A^2 = k^2 - k_0^2 \varepsilon_{mA}$. We have ignored the $\exp(-\beta_A z)$, $\beta_A \in \mathbb{R}_{>0}$ solution because it diverges in the region $z \leq 0$. Substitution of Eq. (10) to Eq. (9) gives

$$E_x(z) = \frac{i\beta_A}{k} E_A \exp(\beta z), \qquad \beta_A \in \mathbb{R}_{>0}.$$

(ii) Solution of Eq. (6) *in region* **B** *where* $0 < z \leq d_1$ *:*

The presence of the electrical field in the Schottky junction has completely depleted the free carriers in the region **B**, and thus the permittivity is constant and given by the Eq. (4b). Therefore, as in the region **A**, we get the following simplified version of Eq. (6),

$$\frac{\partial^2 E_z}{\partial z^2} + (k_0^2 \varepsilon_{sB} - k^2) = 0,$$

which has the following general solution

$$E_z(z) = E_{B1} \cos(\beta_B z) + E_{B2} \sin(\beta_B z), \qquad \beta_B \in \mathbb{R}_{\geq 0} \tag{11}$$

where $\beta_B^2 = k^2 - k_0^2 \varepsilon_{sB}$ and E_{B1} and E_{B2} are constants. We keep the most general solution here because the boundary conditions are finite and hence the general solution never diverges within the region of interest. Substitution of Eq. (11) to Eq. (9) gives

$$E_x(z) = \frac{i\beta_B}{k}(-E_{B1} \sin(\beta_B z) + E_{B2} \cos(\beta_B z)).$$

#161732 - $15.00 USD Received 18 Jan 2012; revised 28 Feb 2012; accepted 5 Mar 2012; published 13 Mar 2012

(iii) Solution of Eq. (6) *in region* **C** *where* $d_1 < z \leq d_2$ *:*

The carrier density is assumed to vary linearly in this section as shown in Fig. 2. This carrier density dependency translates to the variation of the permittivity as shown in Eq. (4c). Substitution of the permittivity variation to Eqs. (6) and (7) result in the following equations:

$$\frac{\partial^2 E_z(z)}{\partial z^2} + \frac{1}{(z-z_0)}\frac{\partial E_z(z)}{\partial z} - \left[k^2 + \frac{\varepsilon_{Hs} r \omega_{ps0}^2}{c^2}(z-z_0) + \frac{1}{(z-z_0)^2}\right] E_z(z) = 0 \tag{12}$$

$$E_x(z) = \frac{i}{k}\left[\frac{\partial E_z(z)}{\partial z} + \frac{E_z(z)}{(z-z_0)}\right] \tag{13}$$

Noting that when $d_1 < z \leq d_2$, the inequality $\frac{\varepsilon_{Hs} r \omega_{ps0}^2}{c^2}(z-z_0)^3 + 1 \gg k^2(z-z_0)^2$, we get

$$\frac{\partial^2 E_z(z)}{\partial z^2} + \frac{1}{(z-z_0)}\frac{\partial E_z(z)}{\partial z} - \left[\frac{\varepsilon_{Hs} r \omega_{ps0}^2}{c^2}(z-z_0) + \frac{1}{(z-z_0)^2}\right] E_z(z) = 0$$

This equation has the following analytical solution

$$E_z(z) = \frac{E_{C1}}{z-z_0}\,\mathrm{Ai}'\left(\frac{z-z_0}{\xi}\right) + \frac{E_{C2}}{z-z_0}\,\mathrm{Bi}'\left(\frac{z-z_0}{\xi}\right) \tag{14}$$

where E_{C1} and E_{C2} are constants, $\mathrm{Ai}'(z)$ is the first derivative of the Airy function with respect to the variable z [22], $\mathrm{Bi}'(z)$ is the first derivative of the Bairy function with respect to the variable z and $\xi^3 = c^2/\varepsilon_{Hs} r \omega_{ps0}^2$. Substitution of Eq. (14) to Eq. (13) gives,

$$E_x(z) = \frac{i}{k}\left[\frac{E_{C1}}{\xi^2}\,\mathrm{Ai}\left(\frac{z-z_0}{\xi}\right) + \frac{E_{C2}}{\xi^2}\,\mathrm{Bi}\left(\frac{z-z_0}{\xi}\right)\right]$$

(iv) Solution of Eq. (6) *in region* **D** *where* $z > d_2$ *:*

Here the dielectric function is spatially constant (see Eq. (4d)) and hence Eq. (6) assumes the following simple form:

$$\frac{\partial^2 E_z}{\partial z^2} + (k_0^2 \varepsilon_{sD} - k^2) = 0 \tag{15}$$

As in the region **A** the solution of the Eq. (15) is well-known and can be written directly as

$$E_z(z) = E_D \exp(-\beta_D z), \qquad \beta_D \in \mathbb{R}_{>0}, \tag{16}$$

where E_D is a constant and the longitudinal wave vector is given by $\beta_D^2 = k^2 - k_0^2 \varepsilon_{sD}$. We have ignored the $\exp(\beta_D z), \beta_D \in \mathbb{R}_{>0}$ solution because it diverges in the region $z > d_2$. Substitution of Eq. (16) to Eq. (9) gives

$$E_x(z) = -\frac{i\beta_D}{k} E_D \exp(-\beta_D z), \qquad \beta_D \in \mathbb{R}_{>0}.$$

2.3. Surface plasmon dispersion relation

The dispersion relation for the Schottky junction relates the angular frequency, ω of the SPP field to its wave vector magnitude, k. The allowed values of this relationship determine the SPP modes that are supported on the Schottky junction. The dispersion relation can be found by applying self-consistent boundary conditions at $z = 0$, $z = d_1$ and $z = d_2$ to ensure the continuity of electromagnetic field components E_x and H_y, as required by Maxwell's equations. As in the

#161732 - $15.00 USD Received 18 Jan 2012; revised 28 Feb 2012; accepted 5 Mar 2012; published 13 Mar 2012

Fig. 2, the carrier density slope and vertical intersect in region **C** can be derived from d_1 and d_2 where $r = 1/(d_2 - d_1)$ and $\varsigma = -d_1/(d_2 - d_1)$. The application of the boundary conditions leads to

$$\mathbf{M}_{6\times6}(\omega,k)\mathbf{E}_{6\times1} = 0$$

where $\mathbf{M}_{6\times6}(\omega,k)$ is a 6×6 square–matrix,

$$\mathbf{M}_{6\times6}(\omega,k) = \begin{bmatrix} \varepsilon_{mA}(\omega) & -\varepsilon_{Hs} & 0 & 0 & 0 & 0 \\ \beta_A & 0 & -\beta_B & 0 & 0 & 0 \\ 0 & \cos(\beta_B d_1) & \sin(\beta_B d_1) & -E^c_{z1}(d_1) & -E^c_{z2}(d_1) & 0 \\ 0 & -\beta_B \sin(\beta_B d_1) & \beta_B \cos(\beta_B d_1) & -E^c_{x1}(d_1) & -E^c_{x2}(d_1) & 0 \\ 0 & 0 & 0 & E^c_{z1}(d_2) & E^c_{z2}(d_2) & -\exp(-\beta_D d_2) \\ 0 & 0 & 0 & E^c_{x1}(d_2) & E^c_{x2}(d_2) & \beta_D \exp(-\beta_D d_2) \end{bmatrix}$$

and $\mathbf{E}_{6\times1} = [E_A, E_{B_1}, E_{B_2}, E_{C_1}, E_{C_2}, E_D]^T$ is a 6×1 column–matrix containing undermined coefficients of the solutions given in Eqs. (10), (11), (14) and (16). The matrix elements, $E^c_{z1}(z)$, $E^c_{z2}(z)$, $E^c_{x1}(z)$ and $E^c_{x2}(z)$ are defined using the Airy function, $\mathrm{Ai}(z)$, derivative of Airy function $\mathrm{Ai}'(z)$, Airy function of the second kind, $\mathrm{Bi}(z)$ and its derivative $\mathrm{Bi}'(z)$ as follows:

$$E^c_{z1}(z) = \frac{1}{z-z_0}\,\mathrm{Ai}'\left(\frac{z-z_0}{\xi}\right),$$
$$E^c_{z2}(z) = \frac{1}{z-z_0}\,\mathrm{Bi}'\left(\frac{z-z_0}{\xi}\right),$$
$$E^c_{x1}(z) = \frac{i}{k}\left[\frac{1}{\xi^2}\,\mathrm{Ai}\left(\frac{z-z_0}{\xi}\right)\right],$$
$$E^c_{x2}(z) = \frac{i}{k}\left[\frac{1}{\xi^2}\,\mathrm{Bi}\left(\frac{z-z_0}{\xi}\right)\right].$$

In order to obtain a non trivial solution for the coefficient matrix $\mathbf{E}_{6\times1}$ for permissible $\{\omega,k\}$ values, the determinant of the matrix, $\mathbf{M}_{6\times6}(\omega,k)$ must be equal to zero. This condition results in a secular equation relating ω and k; which is the dispersion relation for the Schottky junction:

$$\text{Dispersion Relation of the Schottky Junction:} \qquad \mathrm{Det}(\mathbf{M}_{6\times6}(\omega,k)) = 0$$

The compact form of this dispersion relation enable us to carry out normally computationally expensive studies involving the Schottky junction with much ease. For example, the solutions of the dispersion relation can be used to study plasmonic pulses propagating along the Schottky junction by integrating the corresponding wave equation. Another use of such a solution is to use the values as a initial guess for a high accuracy numerical polishing routine with a nonlinear carrier density profile in the vicinity of the Schottky junction interface.

It is instructive to look at the accuracy of this dispersion relation against a detailed numerical solution constructed using an infinite series for the region **C**. The solutions we previously obtained for regions **A**, **B** and **D** are exact and hence do not need any numerical refinement. Based on the work of Frobenius [23], we assume that the Eq. (12) has an infinite series in the following form

$$E_z(z) = (E_{CF1} + E_{CF2}\ln|z-z_0|)\sum_{n=0}^{\infty} u_n (z-z_0)^{n-1} + E_{CF2}\sum_{n=0}^{\infty} v_n (z-z_0)^{n-1} \qquad (17)$$

#161732 - $15.00 USD Received 18 Jan 2012; revised 28 Feb 2012; accepted 5 Mar 2012; published 13 Mar 2012

where E_{CF1} and E_{CF2} are constants to be determined using boundary conditions. Substituting Eq. (17) to Eq. (12) and equating coefficients of the $(z-z_0)^n$ terms to 0, we arrive at following recurve relations for the coefficients of the infinite series:

$$u_0 = 0, \qquad u_1 = 0, \quad u_2 = \frac{k^2}{2}, \qquad\qquad u_n = \frac{k^2 u_{n-2} + \frac{\varepsilon_{Hs} r \omega_{ps0}^2}{c^2} u_{n-3}}{n(n-2)}, \quad n \geq 3$$

$$v_0 = 1, \qquad v_1 = 0, \quad v_2 = -\frac{k^2}{4}, \qquad v_n = \frac{-2(n-1)u_n + k^2 v_{n-2} + \frac{\varepsilon_{Hs} r \omega_{ps0}^2}{c^2} v_{n-3}}{n(n-2)}, \quad n \geq 3.$$

Substitution of Eq. (17) to Eq. (13) gives,

$$E_x(z) = \frac{i}{k}\left(E_{CF1} + E_{CF2}\ln|z-z_0| + \frac{E_{CF2}}{z-z_0}\right)\sum_{n=1}^{\infty} n u_n (z-z_0)^{n-2} + \frac{i}{k} E_{CF2} \sum_{n=1}^{\infty} n v_n (z-z_0)^{n-2}.$$

Figure 3 shows the plasmonic dispersion curves calculated using our Airy function based method and the Frobenius series solution above. We obtained the same result for semiconductor–vacuum interface given in Ref. [20] based on the Frobenius solution. The result in Fig. 3 is obtained for the metal-semiconductor interface for easy comparison. The difference, ω_{diff}, between two solutions is shown in the inset of Fig. 3, which is below 1.0%. This confirms the high accuracy of the analytical dispersion relation and we use it exclusively in the analysis below.

3. Behaviour of SPP modes on the Schottky junction

To gain some insight into the types of modes supported by the Schottky junction depicted in Fig. 2, a set of interesting scenarios are considered in this section. Unless otherwise stated, we assume that the Schottky junction is made by interfacing Gold (Au) to doped Silicon (n–Si) (see Fig. 1). It is known that SPP propagation in multi-layer systems support multiple modes

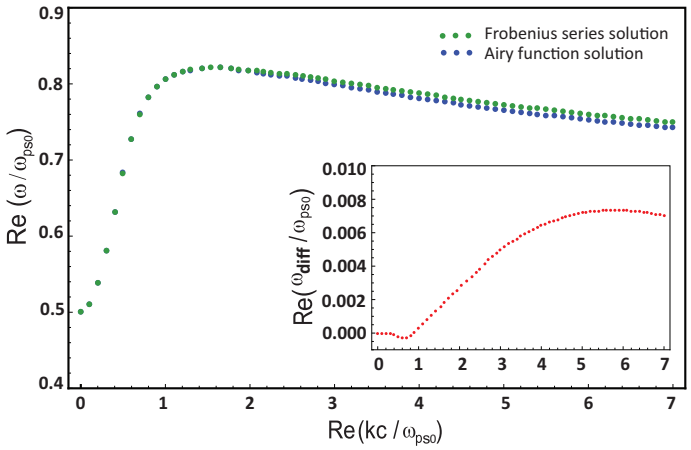

Fig. 3. Plasmonic dispersion curves for a metal–semiconductor interface using our Airy function method and Frobenius series solution method. The difference ω_{diff} between the curves is shown in the inset, which is below 1.0%.

#161732 - $15.00 USD Received 18 Jan 2012; revised 28 Feb 2012; accepted 5 Mar 2012; published 13 Mar 2012

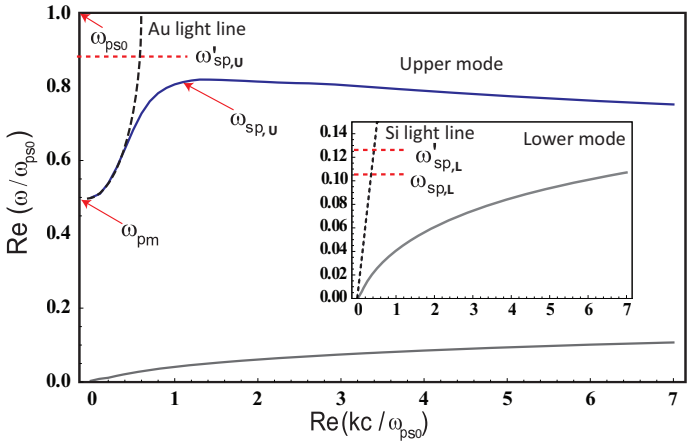

Fig. 4. The dispersion curves of Schottky junction for $\omega_{ps0} = 2\omega_{pm}$. The frequencies marked in the figure are normalized to bulk plasma frequency of the semiconductor. Two dispersion modes are shown where lower mode is magnified in the inset of the figure. The calculations are carried out for $\varepsilon_{Hs} = 11.9$, $\omega_{pm} = 1.36 \times 10^{16} rad/s$ and d_1, d_2 values are taken for doping concentration of $10^{-28} m^{-3}$.

depending on layer widths [24]. Here we noted two surface plasmon modes for the Schottky junction at high frequency and low frequency regions. The two modes are plotted in Fig. 4 where the low frequency mode is magnified in the inset. The lower mode behaves similar to the SPP dispersion of metal-dielectric system where it stays right to the bulk Si light line and level off at asymptotic value $\omega_{sp,L}$. The high frequency mode is more similar to the SPP dispersion of a bi-metallic system, where this mode only supports in between bulk plasma frequencies of the metal and the semiconductor. The mode starts from plasma frequency of the metal rising parallel to Au light line and reaches the asymptotic value $\omega_{sp,U}$ thereafter showing a slight negative slope. The limiting conditions for the two modes can be defined when $d_2 \to 0$ and $d_1 \to \infty$. When $d_2 \to 0$, the space charge layer vanishes and creates a bi-metallic interface. Therefore the asymptotic value of upper mode (high frequency mode) is always $\omega_{sp,U} \leq \omega'_{sp,U}$. When $d_1 \to \infty$, the metal-dielectric interface dominates. Hence asymptotic value of lower mode (low frequency mode) is always $\omega_{sp,L} \leq \omega'_{sp,L}$. Here $\omega'_{sp,U}$ and $\omega'_{sp,L}$ are defined as [25],

$$\omega'_{sp,U} = \sqrt{\frac{\omega_{pm}^2 + \varepsilon_{Hs}\omega_{ps0}^2}{(1+\varepsilon_{Hs})}}$$

$$\omega'_{sp,L} = \sqrt{\frac{\omega_{pm}^2}{(1+\varepsilon_{Hs})}}$$

A set of dispersion curves are depicted in Figs. 5–7 to illustrate the effect of free carrier charge density profiles, applied voltage and plasma frequency for the SPP dispersion in a Schottky junction. The carrier density profile decides the d_1 and d_2 values of the junction (cf. Fig. 2). As in Fig. 5(a), the negative slope of the upper mode can be controlled by changing d_1 and d_2. The negative slope increases when d_1 is increased while d_2 is decreased. In contrast, the upper level of low frequency mode decreases when d_1 is increased and d_2 is decreased (see Fig. 5(b)). Also an externally applied potential can be used to control the width of the space charge layer according to Eq. (1), which is considered to be the major advantage of our model. By increasing the reverse biased potential, values of d_1 and d_2 can be shifted by similar amount and

#161732 - $15.00 USD Received 18 Jan 2012; revised 28 Feb 2012; accepted 5 Mar 2012; published 13 Mar 2012

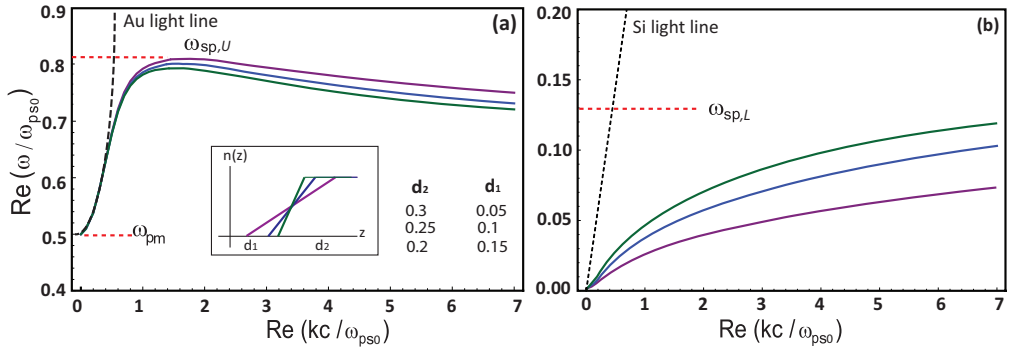

Fig. 5. Dispersion curves for varying carrier density profiles shown in the inset. (a) variation of upper modes with slope r and (b) variation of lower modes with slope r. The frequencies marked in the figure are normalised to bulk plasma frequency of the semiconductor, ω_{ps0} and d_1, d_2 values are normalised by c/ω_{ps0}.

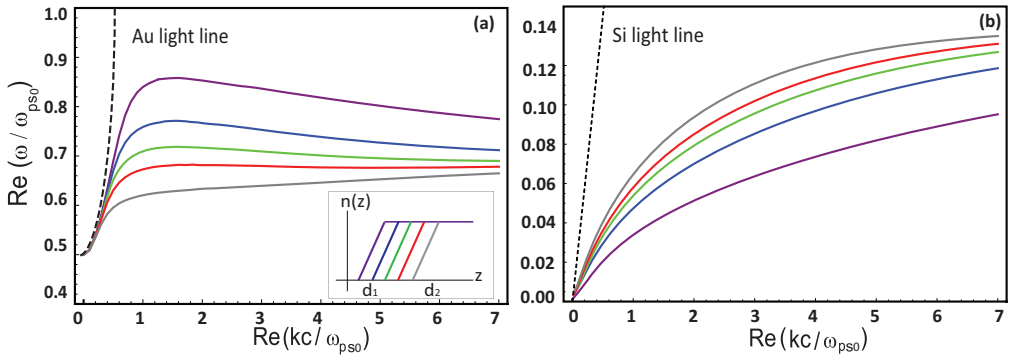

Fig. 6. Dispersion curves for different space charge layer widths by varying externally applied potential. (a) Upper modes for different d_1 and d_2 values as in the inset. (b) Lower modes for different d_1 and d_2 values as in the inset of (a) The values of d_1 and d_2 vary by 0.1 steps starting from 0.05 and 0.1 respectively. The frequencies marked in the figure are normalised to bulk plasma frequency of the semiconductor, ω_{ps0} and d_1, d_2 values are normalised by c/ω_{ps0}.

accordingly the maximum level of two modes can be shifted along the frequency axis (see Figs. 6(a) and 6(b)). Moreover, the externally applied potential can cause to bend the energy band at the semiconductor surface downward or upward creating accumulation or inversion layer depending on forward or reverse biased conditions, respectively. The dispersion characteristics for these conditions can also be found using a similar approach where accumulation layer reduces our model into three layers while inversion layer replaces it with five layers. The plasma frequency of metal decides frequency margin values for the upper mode and also controls the maximum level of the lower mode as illustrated in Figs. 7(a) and 7(b). Altogether, it is clear that the space charge layer formed in a Schottky junction plays a significant role on its SPP dispersion characteristics with more controllability compared to the SPP modes of conventional metal-dielectric interfaces.

Now consider the scenario where the dielectric function ε_{mA} of the metal is complex. The imaginary part of the dielectric constant is responsible for the losses seen by the SPPs, makes

#161732 - $15.00 USD Received 18 Jan 2012; revised 28 Feb 2012; accepted 5 Mar 2012; published 13 Mar 2012

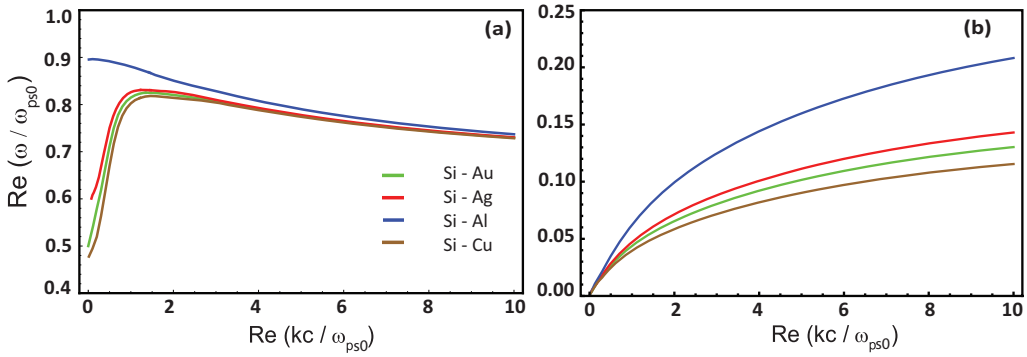

Fig. 7. Dispersion curves obtained using different metals for the Schottky junction: (a) Upper modes and (b) Lower modes. Each upper mode curve starts from the bulk plasma frequency of the particular metal. The frequencies marked in the figure are normalised to bulk plasma frequency of the semiconductor, ω_{ps0}.

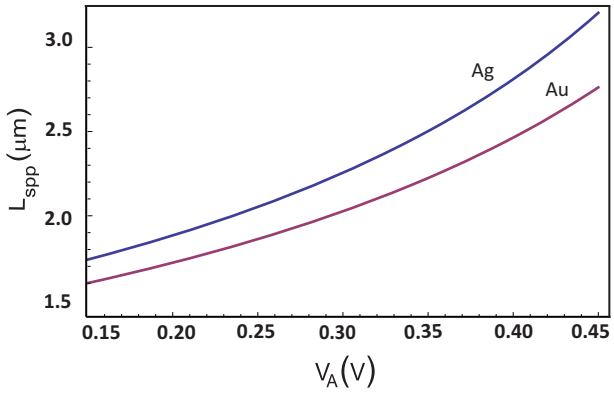

Fig. 8. Dependence of effective propagation length of the plasmon mode with varying forward biased voltage across the Schottky junction. The attenuation coefficients of Au and Ag at $\omega = 1.1 \times 10^{15}\ rad/s$ are $7.953 \times 10^5\ cm^{-1}$ and $7.542 \times 10^5\ cm^{-1}$.

the SPP wave vector complex valued. The imaginary part of this SPP wave vector k_{img} and associated mode propagation length L_{spp} can be found using attenuation coefficient of the metal α_m and optical gain coefficient of the semiconductor $g(n)$, where n denotes the minority carrier concentration:

$$L_{spp} = \frac{1}{2k_{img}} = \frac{1}{\alpha_m - g(n)}$$

Here $g(n) = g_o(n - n_t)$ where g_o and n_t are the gain constant and the transparency density. These two constants are calculated numerically by solving the one-electron model which defines the optical gain with band to band transition of the semiconductor [11, 26]. Also the variation of SPP propagation length with the externally applied voltage is analysed for two different metals as depicted in Fig. 8. As is apparent, the propagation length increases with the biased voltage which has defined below the breakdown voltage of the semiconductor. Here we used n-type $Ga_{0.47}In_{0.53}As$ for the semiconductor material for easy comparison of the results obtained with reference [11]. At $\omega = 1.1 \times 10^{15} rad/s$, the attenuation coefficients of Au and Ag are $7.953 \times 10^5\ cm^{-1}$ and $7.542 \times 10^5\ cm^{-1}$ while the constants g_o and n_t are found to be

#161732 - $15.00 USD Received 18 Jan 2012; revised 28 Feb 2012; accepted 5 Mar 2012; published 13 Mar 2012

$8.76 \times 10^{-16} cm^2$ and $3.7 \times 10^{16} cm^{-3}$. So when the forward biased voltage across the junction increases, the width of space charge layer decreases (as in Eq. (1)) and under certain conditions set by the energy bands, it causes an inversion layer to be formed. It means the minority carrier concentration near the contact exceeds the majority carrier concentration leading to reduction of losses seen by the SPP field (Ref. [11, 26]). In other words, we can control the losses seen by the SPP field by changing the space charge layer width using an external voltage and thus effectively gaining the ability to control the mode propagation length.

4. Conclusion

We derived a highly accurate (i.e. within 1% of the full numerical solution) analytical dispersion relation for surface plasmon modes on a Schottky junction interface. Our derivation takes into account the appearance of the depletion region in the vicinity of the junction and the resulting nonuniform permittivity along the depletion region. The compact form of this dispersion relation enable us to carry out normally computationally expensive studies involving the Schottky junction with much ease. For example, the solutions of the dispersion relation can be used to study plasmonic pulses propagating along the Schottky junction by integrating the corresponding wave equation. Another use of such a solution is to use the values as an initial guess for a high accuracy numerical polishing routine with a nonlinear carrier density profile in the vicinity of the Schottky junction interface. Unlike a metal- dielectric interface which supports a single SPP mode, we found that the Schottky junction is able to support two basic SPP modes, that are termed upper mode and lower mode. The upper mode behaves very similar to a SPP mode on a bi-metallic interface. In contrast to this, the lower mode behaves much more like a SPP mode on a metal-dielectric interface. It is interesting to note that the two modes obtained in this paper for the plasmon dispersion in a Schottky junction are qualitatively in agreement with the results of Inkson [17]. Moreover, the effects of charge density profile, plasma frequency of metal and externally applied potential on dispersion characteristics were also discussed. The charge density profile controls the negative slope of the upper mode curve and bulk plasma frequency controls the frequency margins of the two modes. It was found that using an externally applied potential across the junction, the maximum level of two modes can be shifted along the frequency axis. Thus, it is clear that the Schottky junctions provides a greater controllability over SPP modes on its interface compared with the conventional metal–dielectric interfaces. Especially given that a population inversion can be made in the vicinity of the Schottky junction (cf. [11]), it is very likely that SPP waveguides will be made incorporating Schottky junctions for next generation integrated optics/plasmonics applications requiring long propagation distances.

Acknowledgments

The work of M. Premaratne was sponsored by the Australian Research Councils (ARCs) Discovery grant DP110100713. T. Wijesinghe acknowledges financial support from both the Monash Research Graduate School and the Faculty of Engineering, Monash University.

#161732 - $15.00 USD Received 18 Jan 2012; revised 28 Feb 2012; accepted 5 Mar 2012; published 13 Mar 2012